INTERNATIONAL JOURNAL FOR NUMERICAL METHODS IN FLUIDS
Int. J. Numer. Meth. Fluids 2008; **58**:751–780
Published online 17 March 2008 in Wiley InterScience (www.interscience.wiley.com). DOI: 10.1002/fld.1777

A stability analysis of an oscillating body located in fluid flow using automatic differentiation

Masakazu Furumi and Mutsuto Kawahara*, †

Department of Civil Engineering, Chuo University, Kasuga 1-13-27 Bunkyo-ku, Tokyo 112-8551, Japan

SUMMARY

This paper presents a stability analysis of an oscillating body subjected to fluid forces located in a transient incompressible viscous flow. If the body is supported by elastic springs, oscillation will begin. If the characteristic period of the body and the excited oscillating period due to fluid forces match each other, resonance can occur. Stability analysis is therefore needed to determine the nonlinear behavior of the body. This paper presents an analysis of the changing stability of bodies by the numerical computation. To implement the computation, the motion of fluid around a body is expressed by the Navier–Stokes equation described in the arbitrary Lagrangian–Eulerian form. The fluid influence on the body is discretized by the finite element method based on a mixed interpolation by the bubble function in space. The motion of the body is assumed to be expressed by the equations of motion.

To evaluate stability, stability function is defined by the total energy of the oscillating body. The stability is judged according to a stability index, obtained by the use of the automatic differentiation (AD) of the stability function. AD is a derivative computation method that gives high accuracy. By the use of AD, the second-order derivative matrix, which is needed to compute the stability index, can be obtained exactly.

For the numerical studies, analyses of one degree of freedom and two degrees of freedom (2DOF) for a circular cylinder and 2DOF for a rectangular cylinder are carried out. A combination of a cylinder and supporting elastic spring can produce stable, neutral and unstable states. It is shown that the stability of the cylinder can be determined by the stability index. This paper shows new possibilities for stability analysis of bodies located in a fluid flow. Copyright © 2008 John Wiley & Sons, Ltd.

Received 19 February 2007; Revised 10 November 2007; Accepted 2 January 2008

KEY WORDS: stability analysis; automatic differentiation; ALE method; finite element method; bubble function element; energy method

*Correspondence to: Mutsuto Kawahara, Department of Civil Engineering, Chuo University, Kasuga 1-13-27 Bunkyo-ku, Tokyo 112-8551, Japan.
†E-mail: kawa@civil.chuo-u.ac.jp

1. INTRODUCTION

The purpose of this paper is to present a stability analysis of an oscillating body supported by elastic springs located in a 2D transient viscous fluid flow by means of automatic differentiation (AD). Stability analysis is not merely a theoretical approach to fluid mechanics: it also provides important real-world applications over a wide range of engineering fields with numerous practical examples, including the collapse of the Tacoma Narrows Bridge, unusual vibrations of blades in turbines and unforeseen breakdowns of fluid gauges. A rigid body supported by elastic springs and located in a flow oscillates as a result of the fluid force. In this paper, a numerical analysis of the stability of an oscillating body located in a fluid flow is described using an energy method based on the finite element method.

Conventional stability analysis is conducted using eigenvalues and eigenvectors. Previous studies are reviewed in [1–3]. The minimum value of eigenvalue is obtained and stability is judged according to its positive or negative sign. Computing eigenvalues is extremely laborious. Stability can also be analyzed using other methods. One is the method based on the energy derivative, which is called the energy approach. There are no previous papers presented dealing with this approach based on the finite element method. In this paper, a stability analysis based on the energy derivative using the AD is presented.

To express the movement of a rigid body, the arbitrary Lagrangian–Eulerian (ALE) finite element method is used in the analysis. For the temporal discretization of the velocity of the momentum equation, the Crank–Nicolson method is applied to obtain the implicit scheme and the pressure equation explicit method is employed. The stabilized bubble function finite element method is used to stabilize the computation. Mesh control is one of the most important and difficult challenges in the ALE method. Traditional mesh control methods are unsuitable because of mesh distortion by large displacements. In this study, assuming small mesh deformation, the shear slip mesh update method (SSMUM) is adopted for the rotational movement. For the mesh control method of vertical movement, the flexible re-mesh update method (FRUM) developed using a transform of SSMUM is used. Those are the improvements of the procedures presented by Tezduyar and his group [4]. Employing these two mesh control methods allows the mesh to be re-meshed without mesh distortion.

The stability of the behavior of the body is evaluated according to the total energy computed by the displacement from the base level, velocity and power to act on the body. To do this, the stability index is introduced, which is the second-order differentiation of the energy for the judgment of body stability. It is difficult to obtain the second-order partial derivative of the total energy of an oscillating body since the total energy, which is a function of displacement, velocity and internal force and which should be differentiated with respect to coordinates, is a function of time. This is termed the variation of function. Derivation of the second-order variation is a particularly hard task to formulate and to program. Therefore, in this study, the AD, which enables numerical differentiation, is applied to solve this difficulty. Stability of the oscillating body can be evaluated using the determinant of the second-order partial derivative, which is referred to as the stability index.

Several numerical studies are presented in this paper. First, a circular cylinder that has one degree of freedom (1DOF) in the vertical direction is analyzed. A stable pattern of periodic body oscillation behavior is assumed. The body oscillates periodically, assuming a high heavy mass and a strong spring support. The body is stable over all time durations. The next study is a pattern comprising weakly elastically supported body oscillation. The body is supported by a weak elastic

DOI: 10.1002/fld

spring and is thus easily moved. The stability index shows close to stable state during semi-periodic oscillation. However, it is revealed that at some points, stability is changed by the stability index. At these points, the forces applied to the body are equilibrated at an instant. This state should correspond to a neutral pattern. The third is a pattern of non-convergence of body oscillation. The body has a very low mass and is supported by a medium-range elastic spring. As the amplitude of oscillation becomes greater and greater, the stability state changes from stable to unstable. An incremental oscillation of the body occurs with the amplitude ultimately increasing toward infinity. Circular and rectangular cylinders that have two degrees of freedom (2DOF) in the vertical and rotational directions are analyzed. Because of the 2DOF, the body oscillation becomes more complex. The stability of the body with respect to irregular oscillation is analyzed using the ALE method and judged by the stability index obtained by the second-order automatic differentiation (SOAD).

2. GOVERNING EQUATION DESCRIBED BY ALE

2.1. Navier–Stokes equation

Consider a 2D circular cylinder located in an unsteady transient flow, assumed to be an elastically supported rigid body. The motion of incompressible viscous flow is described by the non-dimensional Navier–Stokes equation based on the ALE description [5–9]. Let Γ denote the boundary of Ω as shown in Figure 1 and assume that an incompressible viscous flow occupies Ω. The state equation of the flow can be expressed using the following Navier–Stokes equation in the non-dimensional form:

$$\frac{\partial \mathbf{u}}{\partial t}+\mathbf{b}\cdot\nabla\mathbf{u}+\nabla p-v\nabla\cdot(\nabla\mathbf{u}+(\nabla\mathbf{u})^{\mathrm{T}})=\mathbf{f} \quad \text{in } \Omega \tag{1}$$

$$\nabla\cdot\mathbf{u}=0 \quad \text{in } \Omega \tag{2}$$

where $\mathbf{u}$, p and v are, respectively, velocity, pressure and viscosity in which v is the inverse of the Reynolds number. The ALE advection term in the ALE coordinate system is denoted by $\mathbf{b}$ and is expressed as

$$\mathbf{b}=\mathbf{u}-\bar{\mathbf{u}} \tag{3}$$

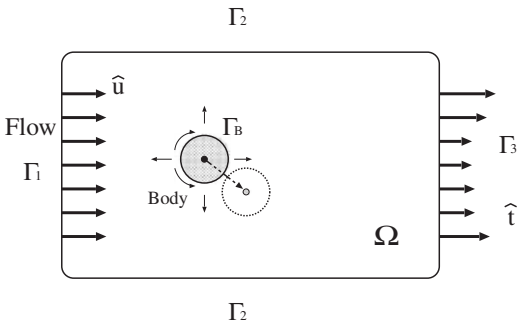

Figure 1. Analysis domain.

DOI: 10.1002/fld

where $\overline{\mathbf{u}}$ is the reference velocity. Because an arbitrary nodal coordinate can be selected in the ALE method, $\overline{\mathbf{u}}$ is expressed by the time derivative of coordinate $\boldsymbol{\chi}$ as

$$\overline{u}=\frac{\hat{\partial}\boldsymbol{\chi}}{\partial t} \tag{4}$$

where $\boldsymbol{\chi}$ is the reference coordinate.

A solid body B with the boundary Γ_B is laid in an external flow; the initial conditions for velocity and pressure are

$$\mathbf{u}=\hat{\mathbf{u}}^{\mathbf{0}} \quad \text{at } t=0 \tag{5}$$

$$p=\hat{p}^0 \quad \text{at } t=0 \tag{6}$$

where $\hat{\mathbf{u}}$ is the constant inflow velocity. The boundary condition is given as follows:

$$\mathbf{u}=(\hat{u},0) \quad \text{on } \Gamma_1 \tag{7}$$

$$\mathbf{u}_2=0, \quad t_1=0 \quad \text{on } \Gamma_2 \tag{8}$$

$$\mathbf{t}=\hat{\mathbf{t}}=0 \quad \text{on } \Gamma_3 \tag{9}$$

$$\mathbf{u}=\mathbf{u}_B \quad \text{on } \Gamma_B \tag{10}$$

$$\mathbf{t}=\{-p\mathbf{I}+\nu(\nabla\mathbf{u}+\nabla\mathbf{u})\}\cdot\mathbf{n} \tag{11}$$

where $\mathbf{t}$ is traction and $\mathbf{n}$ is unit vector of outward normal to Γ, respectively, and $\mathbf{u}_B$ means velocity on boundary Γ_B.

The fluid forces acting on the body are denoted by $\mathbf{F}$, where the three components are drag, lift and momentum forces, respectively. The drag and lift forces in $\mathbf{F}$ are denoted by $\mathbf{F}_{xy}$ obtained by integrating the traction $\mathbf{t}$ over the boundary Γ_B:

$$\mathbf{F}_{xy}=-\int_{\Gamma_B}\mathbf{t}\,\mathrm{d}\Gamma \tag{12}$$

2.2. *Body oscillation*

The body supported by elastic springs shown in Figure 2 in the flow is regarded as a rigid body, is assumed to have three independent DOF and can be described by an equation of body motion. The body has its own acceleration $\{\ddot{X},\ddot{Y},\ddot{\Theta}\}$ and velocity $\{\dot{X},\dot{Y},\dot{\Theta}\}$, where X and Y are displacement movements and Θ is the rotation angle, respectively. The equations of motion are as follows:

$$\mathbf{m}\ddot{\mathbf{X}}+\mathbf{c}\dot{\mathbf{X}}+\mathbf{k}\mathbf{X}=\mathbf{F}_{xy} \tag{13}$$

$$I\ddot{\theta}+c_\theta\dot{\theta}+k_\theta\theta=M \tag{14}$$

where $\mathbf{X}=\{X,Y\}^{\mathrm{T}}$ is the displacement, $\mathbf{F}_{xy}=\{F_x,F_y\}^{\mathrm{T}}$ is the external force, $\mathbf{m}$ is the mass, $\mathbf{c}$ and c_θ are structural dampings, $\mathbf{k}$ and k_θ are spring constants, I is the moment of inertia and M is the moment force applied to the body. The compatibility relationship between rigid body and fluid flow is as follows:

$$\begin{aligned}\dot{\mathbf{u}}^\gamma &= \mathbf{T}^{\mathrm{T}}\ddot{\mathbf{X}}=\mathbf{T}^{\mathrm{T}}\dot{\mathbf{u}}\\ \mathbf{u}^\gamma &= \mathbf{T}^{\mathrm{T}}\dot{\mathbf{X}}=\mathbf{T}^{\mathrm{T}}\mathbf{u}\end{aligned} \tag{15}$$

DOI: 10.1002/fld

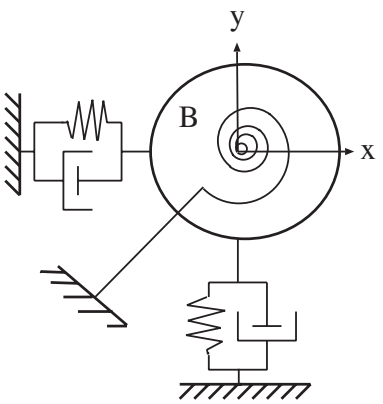

Figure 2. Body support.

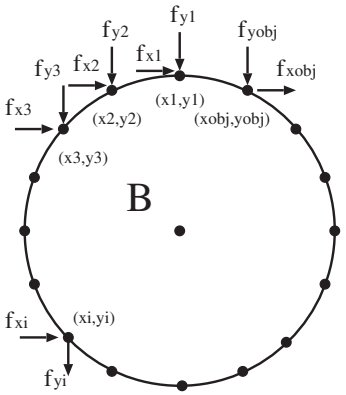

Figure 3. Analytic body.

where superscripted γ means a quantity with respect to the rigid body. The equilibrium condition is expressed as

$$\mathbf{F}+\mathbf{T}\mathbf{f}^{\gamma}=0 \tag{16}$$

where $\mathbf{F}=\{\mathbf{F}_{xy}, M\}^{\mathrm{T}}$ is the fluid force acting on the body and matrix $\mathbf{T}$ expresses the geometric relationship between the center of gravity on the body and each node of the material surface. Figure 3 shows the geometric relation of each node of a circular cylinder, where obj is the number of nodes on the boundary of the circular cylinder. Transformation matrix $\mathbf{T}$ is

$$\mathbf{T}=\begin{bmatrix} 1 & 0 & & 1 & 0 & & 1 & 0 \\ 0 & 1 & \cdots & 0 & 1 & \cdots & 0 & 1 \\ -L_{y_1} & L_{x_1} & & -L_{y_i} & L_{x_i} & & -L_{y_{\mathrm{obj}}} & L_{x_{\mathrm{obj}}} \end{bmatrix}$$

DOI: 10.1002/fld

where

$$\begin{Bmatrix} L_{x_i} \\ L_{y_i} \end{Bmatrix} = \begin{bmatrix} \cos\theta_s & -\sin\theta_s \\ \sin\theta_s & \cos\theta_s \end{bmatrix} \begin{Bmatrix} x_i \\ y_i \end{Bmatrix}$$

where θ_s is the angle of position. Thus, $\mathbf{F}_{xy}$ and M are influenced by the fluid around a body and are expressed as

$$\mathbf{F}_{xy} = \left\{ \sum_{i=1}^{\text{obj}} f_{x_i}, \sum_{i=1}^{\text{obj}} f_{y_i} \right\}^{\mathrm{T}} \tag{17}$$

$$M = \sum_{i=1}^{\text{obj}} (y_i \cdot f_{x_i} - x_i \cdot f_{y_i}) \tag{18}$$

where x_i and y_i are the position coordinates.

3. DISCRETIZATION

The Navier–Stokes equations are discretized by mixed interpolation using the finite element method. Pressure is discretized by the linear interpolation function, whereas velocity is interpolated by the bubble function. The stabilized bubble function, originated by Matsumoto *et al.* [10, 11], is adopted to stabilize the computation. The finite element equation is expressed as

$$\mathbf{M}\dot{\mathbf{u}} + (\mathbf{S}+\mathbf{D})\mathbf{u} - \mathbf{A}\mathbf{p} = \mathbf{f} \tag{19}$$

$$\mathbf{A}^{\mathrm{T}}\mathbf{u} = 0 \tag{20}$$

where $\mathbf{M}$ is the mass, $\mathbf{D}$ is the diffusion, $\mathbf{S}$ is the advection including material arbitrary velocity $\mathbf{b}$, $\mathbf{p}$ is the pressure and $\mathbf{A}^{\mathrm{T}}$ is the transpose of matrix $\mathbf{A}$. The external force $\mathbf{f}$ is given by Equation (16). The Crank–Nicolson method is applied to the discretization in time for velocity in the momentum equation. For the pressure of momentum equation, an explicit scheme is applied to the temporal discretization:

$$\mathbf{M}\frac{\mathbf{u}^{n+1}-\mathbf{u}^n}{\Delta t} + (\mathbf{S}+\mathbf{D})\mathbf{u}^{n+1/2} - \mathbf{A}\mathbf{p}^{n+1} = \mathbf{f}^n \tag{21}$$

$$\mathbf{A}^{\mathrm{T}}\mathbf{u}^{n+1} = 0 \tag{22}$$

where

$$\mathbf{u}^{n+1/2} = \tfrac{1}{2}(\mathbf{u}^{n+1} + \mathbf{u}^n) \tag{23}$$

From these discretizations, two equation systems should be solved at the same time. The computation can be carried out without giving the pressure boundary condition. Moreover, to conduct large-scale computations, the bi-conjugate gradient method with an element-by-element calculation is adopted.

DOI: 10.1002/fld

4. MESH CONTROL

4.1. The SSMUM

The SSMUM [12, 13], designed to handle certain classes of flow problems with moving boundaries, is applied to the ALE method. This method is adaptable to such problems as regular and large boundary displacement of rotation. If a thin layer of extremely distorted elements is accommodated, limited re-meshing needs to be carried out. SSMUM is able to effectively adjust the significantly distorted mesh problem by a large amount of body movement, avoiding cumbersome procedures using re-meshing processes such as the Laplace equation method [8, 9].

The SSMUM is a mesh re-construction method that combines a region of rigid non-variant element and a layer region of shear-absorbing variable elements. Consider the rotation of the body in Figure 4. The rotating body is embedded in a disk of rigid elements which rotates jointly with the body. These variant regions are immersed in another set of non-variant elements spanning the exterior boundaries, as shown in Figure 5. The thickness of this layer can span one or more elements. Non-variant areas around a rotating body move with the motion of the body. Gradually, a variable area mesh is distorted, followed by rotation. Finally, the mesh in the available area is reconstructed between non-moving areas.

4.2. The FRUM

The FRUM, which is a modification of SSMUM applied to straight movement in a limited space, is carried out for vertical transformation. In this method, mesh distortion is minimized in space that

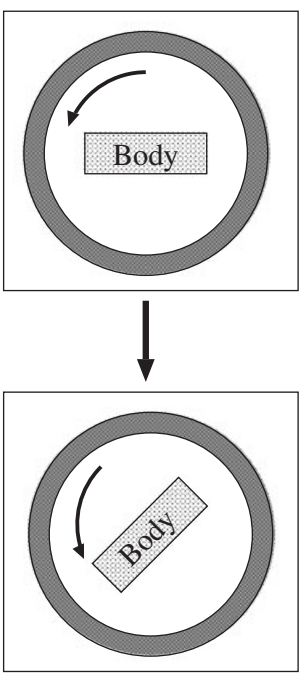

Figure 4. Shear slip model.

DOI: 10.1002/fld

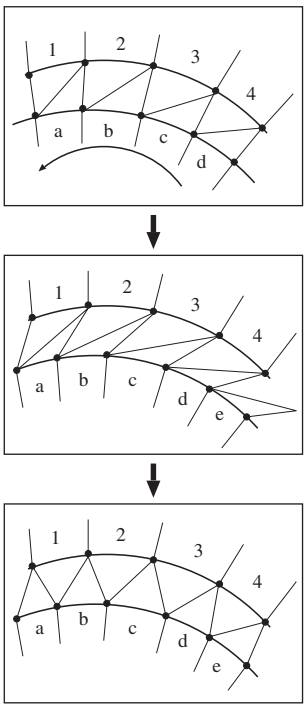

Figure 5. Re-mesh model.

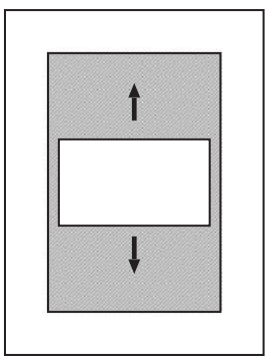

Figure 6. Flexible re-mesh model.

limits one-directional movement to some degree. In this way, re-mesh cost and node movement can be minimized.

The large transformation moving boundary problem can be analyzed using this method, but for only one direction of movement. Application of two different directions in this method and SSMUM to the three degrees of freedom (3DOF) moving boundary problem can be solved in 2D

DOI: 10.1002/fld

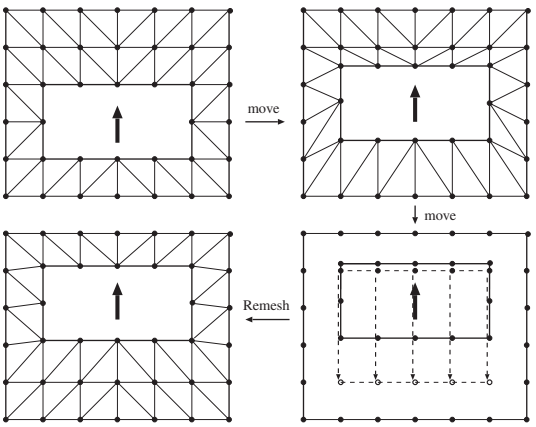

Figure 7. Re-mesh model.

motion. Figure 6 shows the outline of the fixed mesh, moving mesh and flexible re-mesh update (FRU) layers. The fixed mesh has some space for movement of the moving mesh. If the moving mesh is close to the FRU layer node, the FRU layer is reconstructed as shown in Figure 7. In this method, the reconnect criterion is important. The initial width of FRU mesh laid next to the movable mesh is $\mathrm{d}y^0$. Let the width of the FRU mesh after movement lying next to the movable mesh be $\mathrm{d}y^n$. Re-meshing is carried out if

$$\mathrm{d}y^n < C_{\mathrm{RJ}}\,\mathrm{d}y^0 \tag{24}$$

where C_{RJ} is the reconnect criterion. If the moving mesh comes close to the movable nodes, it is necessary to find C_{RJ} so as to minimize mesh distortion between the moving mesh node and the movable nodes. This problem assumes $C_{\mathrm{RJ}}=0.5$, which minimizes the pressed mesh distortion.

5. STABILITY ANALYSIS

A stability criterion depends on its definition. The stability is determined by evaluating the total energy of the oscillating body. The focus of this paper is the total energy of the body located in the incompressible viscous flow and supported by elastic springs that have 3DOF. If the body begins to move, displacement, velocity and acceleration occur. As a result, kinematic energy E_m is generated, which is defined by

$$E_m = \tfrac{1}{2} m U_i^2 + \tfrac{1}{2} I \dot{\Theta}^2 \tag{25}$$

where m is the mass of the body, $U_i = \{U, V\}$, in which U and V are the velocities in the x and y directions, I is the moment of inertia and $\dot{\Theta}$ is the angular velocity of the body's rotation. As the body moves, the elastic springs undergo axial and rotational deformations. As a result, spring energy E_s is generated, which is defined by

$$E_s = \tfrac{1}{2}(k_x X^2 + k_y Y^2 + k_\theta \Theta^2) \tag{26}$$

DOI: 10.1002/fld

where the spring constants in x, y and θ directions are denoted by k_x, k_y and k_θ, respectively, and X, Y and Θ are the body displacements in the x, y and θ directions, respectively.

Owing to the external force applied to the body, potential energy is generated, which is defined by

$$E_p = -\left(\Delta x \sum_{i=1}^{\text{obj}} f_{xi} + \Delta y \sum_{i=1}^{\text{obj}} f_{yi} + \Delta\theta \sum_{i=1}^{\text{obj}} (y_{i0} \cdot f_{xi} - x_{i0} \cdot f_{yi}) \right) \tag{27}$$

where obj is the total number of surface nodes, Δx, Δy and $\Delta\theta$ are the increments of each displacement, f_{x_i} and f_{y_i} are the external forces in the X and Y directions and x_{i0} and y_{i0} are the coordinates at the points of the external forces, respectively.

The total energy E is defined by summation of these energies:

$$E = E_m + E_s + E_p \tag{28}$$

where E is referred to as the stability function. According to the energy theorem, if the energy is positive-definite, then the body motion is stable. To differentiate the total energy by the coordinates of the body node, stability can be evaluated. Second-order differentiation is needed to evaluate the stability of the oscillating body. The evaluation can be performed by AD. Moreover, the determinant of the second-order differentiation needs to be computed to evaluate the stability

$$e = \left| \frac{\partial^2 E}{\partial \mathbf{X}_i \partial \mathbf{X}_j} \right| \tag{29}$$

where e is the stability index, $||$ is the determinant and $\mathbf{X}_i$ is the coordinate on the surface of the body:

$$\mathbf{X}_i = \{x_1, x_2, x_3, \ldots, x_{\text{obj}}, y_1, y_2, y_3, \ldots, y_{\text{obj}}\} \tag{30}$$

where obj is the total number of nodes on the body. The stability is evaluated by the stability index e as follows:

$$e > 0 \quad \text{stable} \tag{31}$$

$$e = 0 \quad \text{neutral} \tag{32}$$

$$e < 0 \quad \text{unstable} \tag{33}$$

6. AUTOMATIC DIFFERENTIATION

Derivatives of functions can be computed precisely not only manually but also by computers. The differentiation rules are defined for each operation in computation. Thus, if a function is described by its computer implementation, it can be differentiated exactly and automatically by overloading operators. This technique is termed AD [14, 15].

It is important to pursue higher-quality computation for partial derivatives in the field of analysis in numerical simulation. Derivatives are computed by using the well-known chain rule for composite

DOI: 10.1002/fld

functions in the normal way. In AD, a function and its derivatives are calculated simultaneously using the same code and common temporary values. If the code for the stability of the function is optimized, then the computation of the derivatives will also be optimized at the same time. There are two types of AD: forward mode and reverse mode.

Forward-mode AD can compute partial derivatives automatically without computational graphs. Therefore, less computational storage is required than with reverse-mode AD. Forward mode AD is therefore used in this paper.

7. NUMERICAL ANALYSIS

7.1. Stability analysis of 1DOF circular cylinder

7.1.1. Stability analysis. The behavior of the circular cylinder's vertical movement is analyzed using the ALE finite element method combined with FRUM. Because of the lift force, the circular cylinder is moved with respect to its center of gravity. It shows a reciprocating up-and-down movement due to incompressible transient viscous flow. Stability analysis is carried out by SOAD. This circular cylinder with 1DOF is analyzed using the different parameters that are listed in Table I. The total energy is defined as follows:

$$E = \tfrac{1}{2} m V^2 + \tfrac{1}{2} k_y Y^2 + E_p \tag{34}$$

and the stability index is

$$e = \left| \frac{\partial^2 E}{\partial \mathbf{X}_i \partial \mathbf{X}_j} \right| \tag{35}$$

where

$$\mathbf{X}_i = \{y_1, y_2, y_3, \ldots, y_{\text{obj}}\} \tag{36}$$

in which $y_1, y_2, y_3, \ldots, y_{\text{obj}}$ are the coordinates on the circular surface of the body.

The computational domain and the finite element mesh are shown in Figures 8 and 9, where the mesh consists of 2720 nodes and 5266 elements, respectively. Boundary conditions are also shown in Figure 8. The Reynolds number is 250. The computations in three cases are carried out corresponding to stable, neutral and unstable states.

The magnitude of the stability index e is not relevant, whereas the information on the sign of the index, positive or negative, is important in determining the stability. Thus, the stability index is plotted in the figures as 0.1 if it is positive, as -0.1 if it is negative, and as 0 if the absolute value of e is small enough, $e < \varepsilon$, where ε is 1.0×10^{-3}.

Table I. Parameters used in computation in cases I, II and III.

Case	Mass		Spring		Time
I	10.0	Heavy	20.0	Strong	60.0
II	1.0	Medium	1.0×10^{-3}	Weak	60.0
III	0.4	Light	0.1	Medium	60.0

DOI: 10.1002/fld

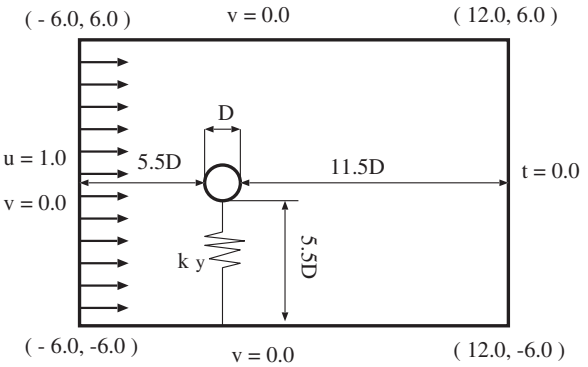

Figure 8. Computational domain.

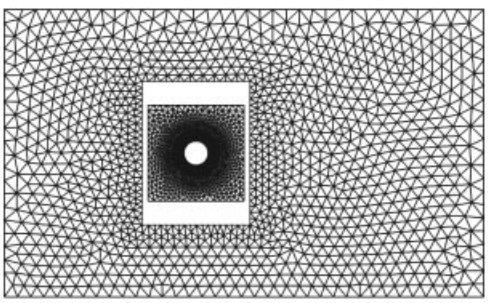

Figure 9. Finite element mesh.

7.1.2. The stable state. The parameters used are as follows: the mass of the circular cylinder is 10.0, the non-dimensional spring constant in the y-direction is 20.0 and the structural damping coefficient is assumed to be 0.0. The time increment, Δt, is 0.02. All values are non-dimensional. The parameters are set with the mass of the circular cylinder being heavy and strong structural springs. The computing time is 0.0–60.0 in non-dimensional time. The numerical results of the stable 1DOF cylinder are illustrated in Figures 10–15.

Figure 10 represents the velocity distribution at non-dimensional time 10. Figure 11 shows the velocity distribution at non-dimensional time 40. The time history of fluid forces around the body is plotted in Figure 12. Figure 13 shows the time history of vertical displacement of the body. Figure 14 is the time history of vertical velocity of the body. The time history of the stability index compared with vertical displacement is shown in Figure 15.

The behavior of the body is classified as stable by the stability index, as shown in Figure 15. During computational time, the stability index shows a stable state. The body oscillation is periodic and its motion is under the control of the elastic spring and fluid flow, suggesting that the body adopts a periodic and stable oscillation; therefore, this condition is referred to as the perfectly stable state.

DOI: 10.1002/fld

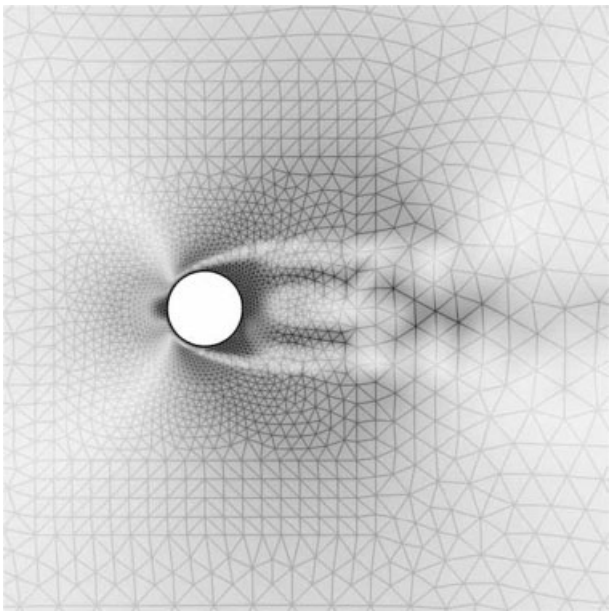

Figure 10. Velocity at time 10 (1D stable circular cylinder).

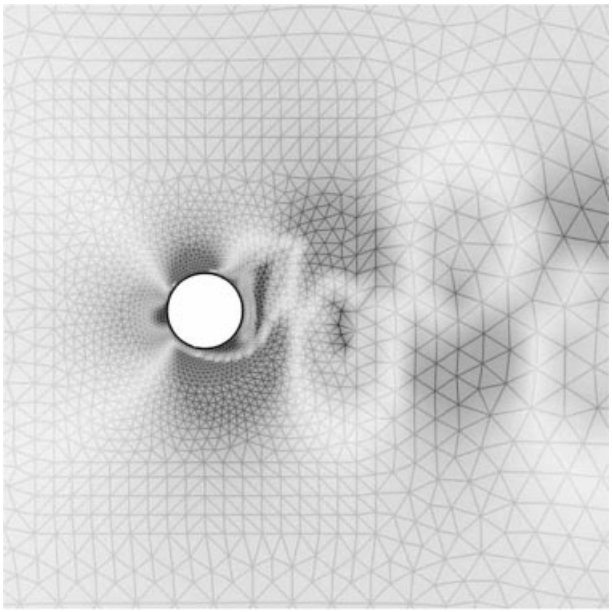

Figure 11. Velocity at time 40 (1D stable circular cylinder).

DOI: 10.1002/fld

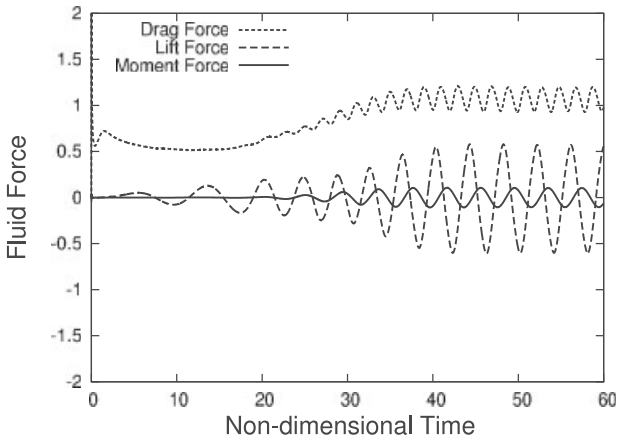

Figure 12. Fluid force *versus* time (1D stable circular cylinder).

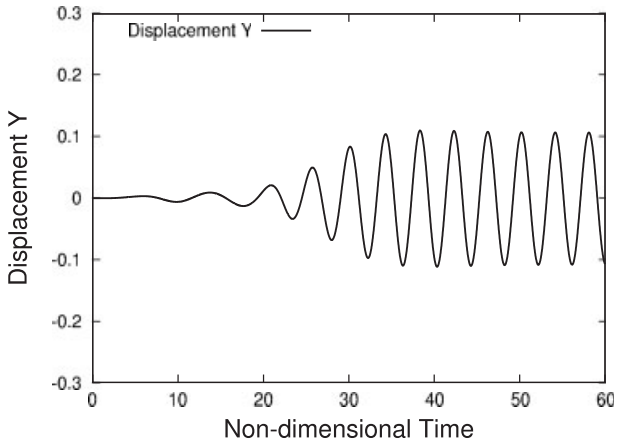

Figure 13. Displacement y of the body *versus* time (1D stable circular cylinder).

7.1.3. The neutral state. The parameters used are as follows: the mass of the circular cylinder is 1.0, the non-dimensional spring constant in the y-direction is 1.0×10^{-3} and the structural damping coefficient is assumed to be 0.0, respectively. The time increment Δt is 0.02. All values are non-dimensional. The parameters set are that the mass of the circular cylinder is medium and the structural spring is weak. The computing time is 0.0–60.0 in non-dimensional time. The numerical results of the neutral 1DOF circular cylinder are shown in Figures 16–21.

Figure 16 represents velocity distribution at non-dimensional time 10. Figure 17 shows velocity distribution at non-dimensional time 40. The time history of the fluid forces around the body is plotted in Figure 18. Figure 19 is the time history of vertical displacement of the body. Figure 20 is the time history of the vertical velocity of the body. The time history of the stability index compared with vertical displacement is shown in Figure 21.

DOI: 10.1002/fld

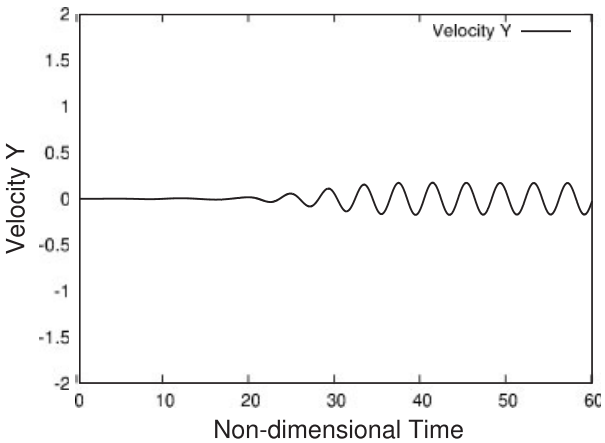

Figure 14. Velocity y of the body *versus* time (1D stable circular cylinder).

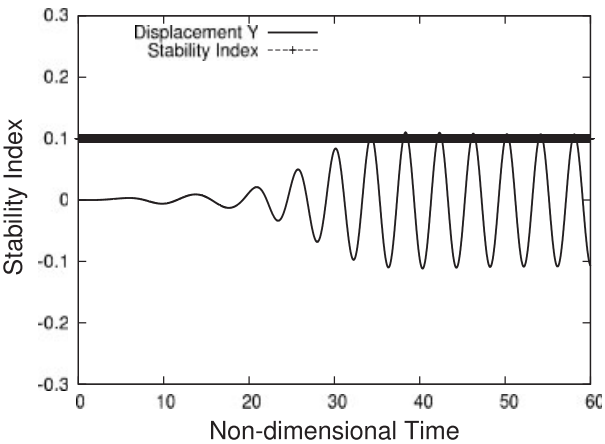

Figure 15. Stability index and y displacement of the body *versus* time (1D stable circular cylinder).

The behavior of the body is classified into two regions according to the stability index, as shown in Figure 21. For the first point, the duration of the neutral region is shown in primary terms by the stability index. The behavior of the stability index shows a constant pattern if the body starts to oscillate. After the neutral region, the stability index shows stability except at some points. Thus, the body begins to start semi-periodic oscillation, and this state is termed the semi-stable oscillation region. Some notable points are included in the semi-stable oscillation region. These are the maximum amplitude neutral points (MANPs). On the maximum amplitude point of semi-periodic oscillation, the stability index shows neutral. MANPs represent the points at which the body is prevented from oscillating because the forces are at equilibrium. This region, where the stability index remains stable except for MANPs, is referred to as the neutral oscillating state.

DOI: 10.1002/fld

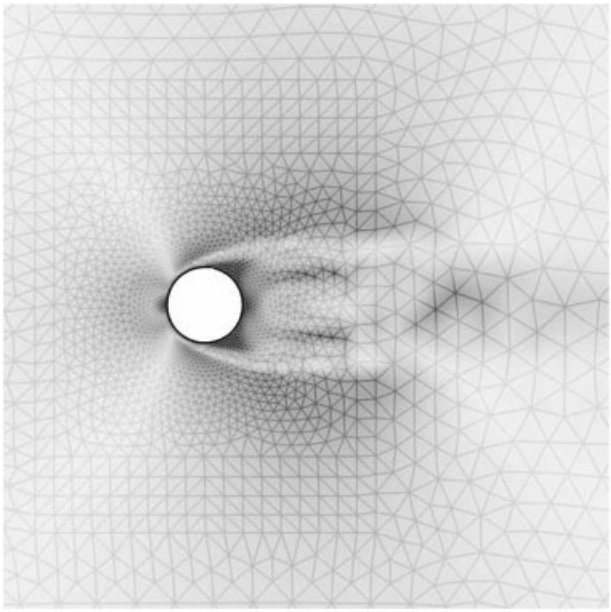

Figure 16. Velocity at time 10 (1D of neutral circular cylinder).

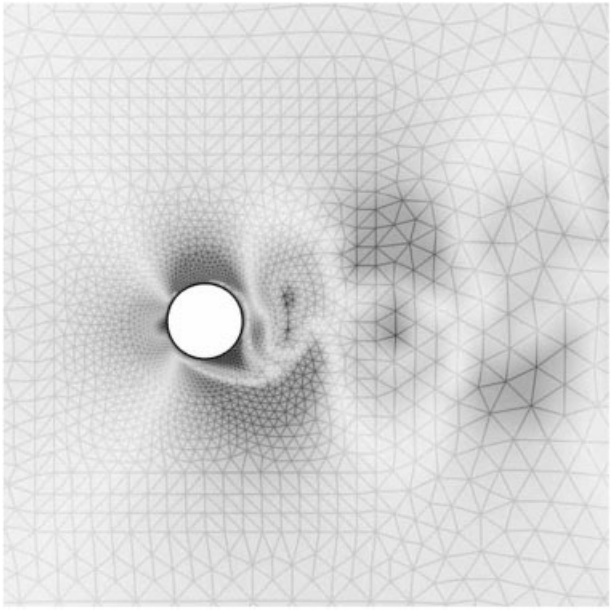

Figure 17. Velocity at time 40 (1D of neutral circular cylinder).

DOI: 10.1002/fld

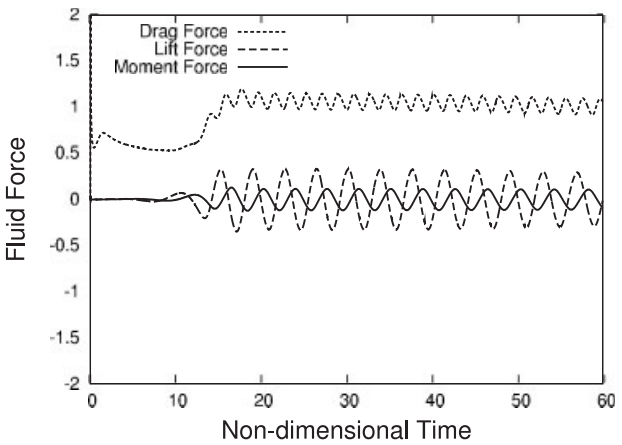

Figure 18. Fluid force *versus* time (1D of neutral circular cylinder).

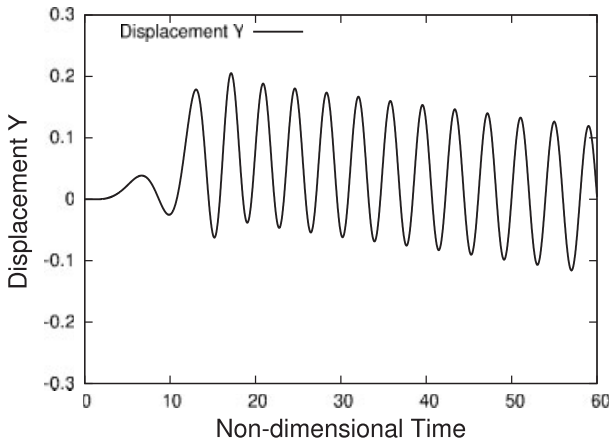

Figure 19. Displacement y of the body *versus* time (1D of neutral circular cylinder).

7.1.4. Unstable state. The parameters used are as follows: the mass of the circular cylinder is 0.4, the non-dimensional spring constant in the y-direction is 1.0×10^{-1} and the structural damping coefficient is assumed to be 0.0. The time increment Δt is 0.02. All values are non-dimensional. The parameters set are that the mass of the circular cylinder is light and the structural spring has medium strength. The computing time is 0.0–60.0 in non-dimensional time. The numerical results of the unstable 1DOF circular cylinder are expressed in Figures 22–27. Figure 22 represents the velocity distribution at non-dimensional time 10. Figure 23 shows velocity magnitude distribution at non-dimensional time 40. The time history of fluid forces around the body is plotted in Figure 24. Figure 25 shows the time history of vertical displacement of the body. Figure 26 is the time history of the vertical velocity of the body. The time history of the stability index compared with vertical displacement is shown in Figure 27.

DOI: 10.1002/fld

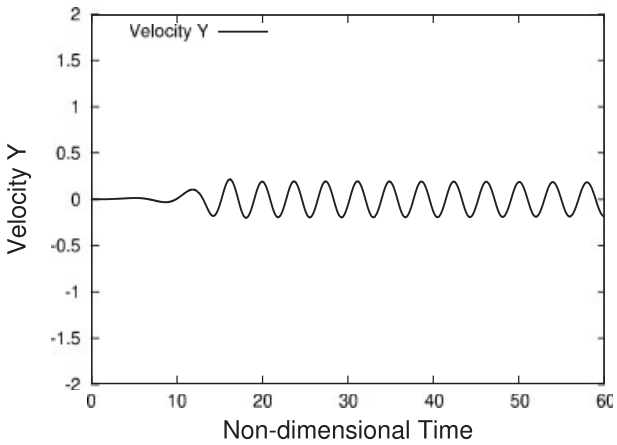

Figure 20. Velocity y of the body *versus* time (1D of neutral circular cylinder).

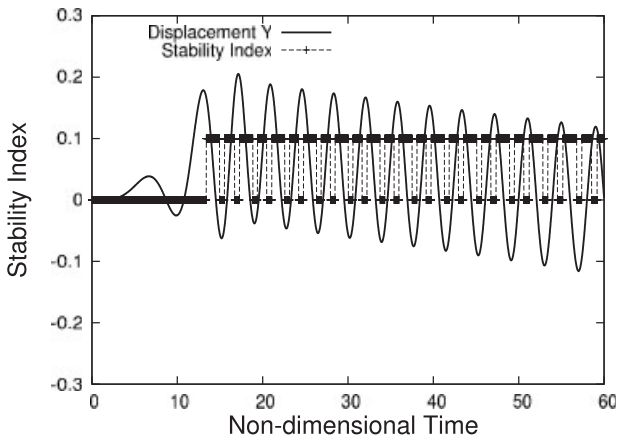

Figure 21. Stability index and y displacement of the body *versus* time (1D of neutral circular cylinder).

The behavior of the body is classified into two regions according to the stability index. The body is supported by a middle-range elastic spring, so that the primary term in oscillation is shown to be stable. However, the body can move easily because of its low mass. The body starts an incremental vibration that is shown in the time history of displacement in Figure 25. Because of incremental vibration, the body velocity dramatically and suddenly changes, as shown in Figure 26. Following the amplification of the body oscillation, the stability transits to the transient stability region, in which the phenomena change from stable to unstable. The body oscillation is gradually amplified and finally exceeds the limit of its stability. The stable body then changes to unstable. Although the body shows low oscillating amplitude immediately afterwards, the body velocity is turned in the opposite direction. For this reason, the body stability immediately changes to unstable. The

DOI: 10.1002/fld

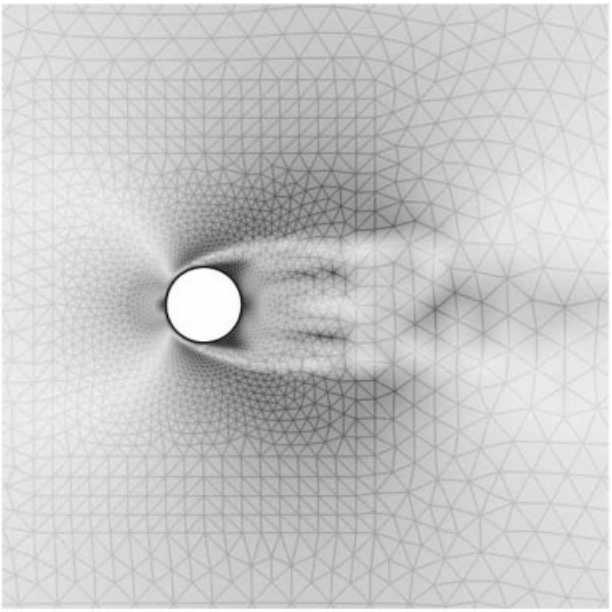

Figure 22. Velocity at time 10 (1DOF unstable circular cylinder).

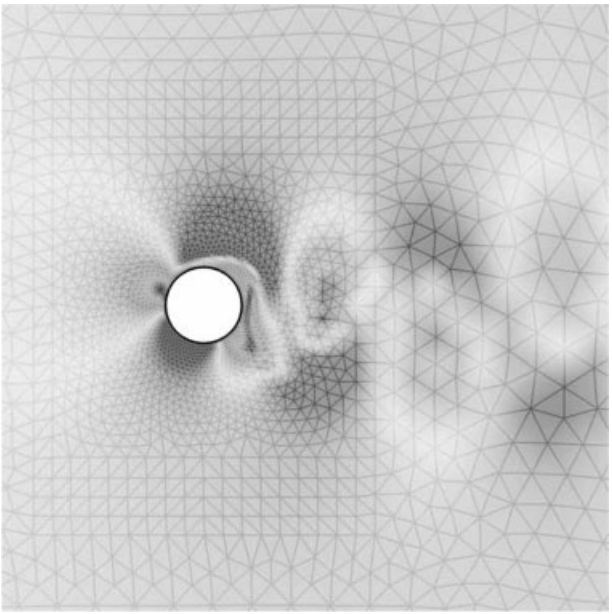

Figure 23. Velocity at time 40 (1DOF unstable circular cylinder).

DOI: 10.1002/fld

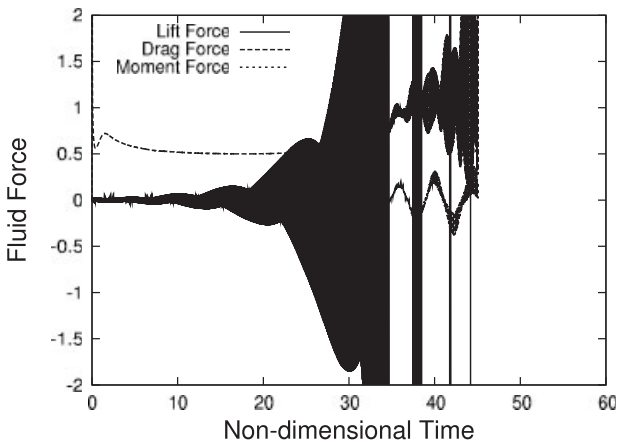

Figure 24. Fluid force *versus* time (1DOF unstable circular cylinder).

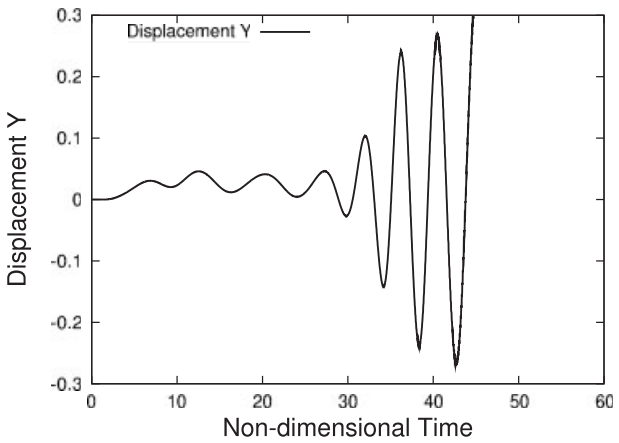

Figure 25. Displacement y of the body *versus* time (1DOF unstable circular cylinder).

body stability of oscillation therefore changes from stable to unstable. Finally, the body oscillation is intensified by the amplification oscillation. In this region, the stability index shows the change from stable to unstable condition; this is referred to as the unstable state.

7.2. Stability analysis of 2DOF circular cylinder

In this study, the behavior of the circular cylinder with 2DOF (rotation and vertical movement) is analyzed by the ALE finite element method combined with SSMUM and FRUM. Because of the lift and moment forces, both the body and its center of gravity move. The motions comprise vibration up and down and rotation with respect to its center of gravity via incompressible transient

DOI: 10.1002/fld

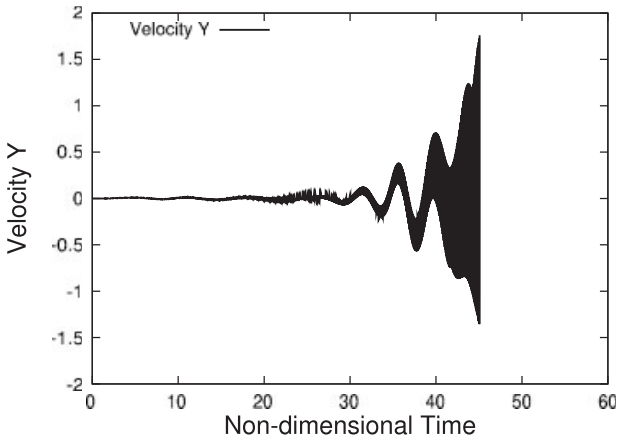

Figure 26. Velocity y of the body *versus* time (1DOF unstable circular cylinder).

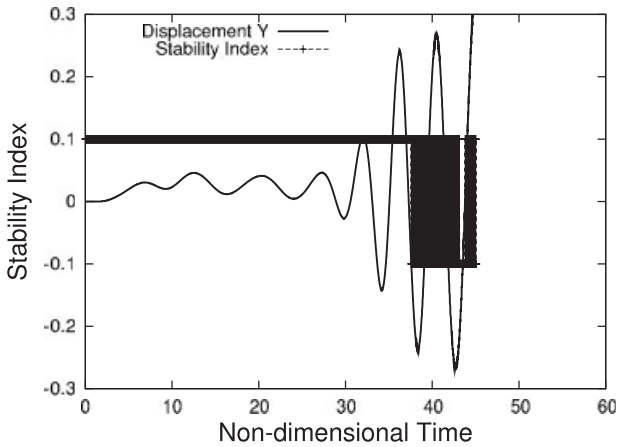

Figure 27. Stability index and y displacement of the body *versus* time (1DOF unstable circular cylinder).

viscous flow. Stability analysis is carried out by the SOAD presented in this paper. The circular cylinder oscillates with 2DOF in this problem. The parameters used are as follows: the mass of the circular cylinder is 1.0, the non-dimensional spring constant in the y-direction is 10.0 and in the θ-direction it is 1.0; the structural damping coefficient is assumed to be 0.0. The time increment Δt is 0.02. All values are non-dimensional. The computing time is 0.0–60.0 in non-dimensional time.

The computational domain and the finite element mesh are shown in Figures 28 and 29, where the mesh consists of 2720 nodes and 5266 elements, respectively. The computational conditions are also shown in Figure 28. The Reynolds number is 250. The numerical results of the 2DOF circular cylinder are expressed in Figures 30–35. Figure 30 represents the velocity distribution at

DOI: 10.1002/fld

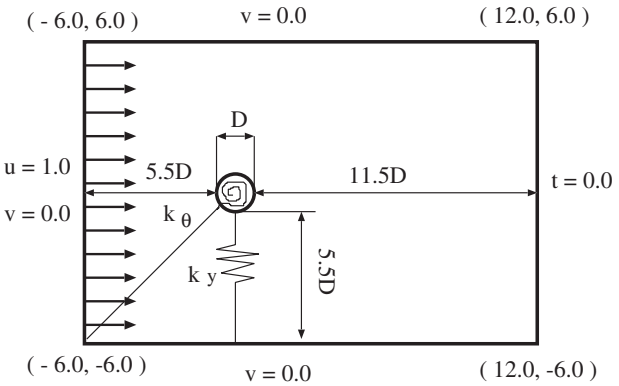

Figure 28. Computational domain.

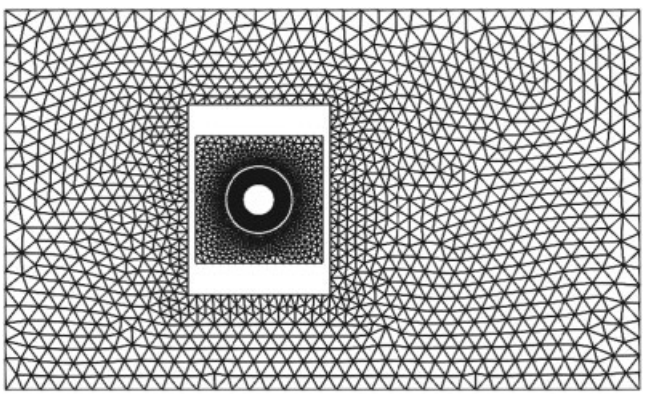

Figure 29. Finite element mesh.

non-dimensional time 10. Figure 31 shows velocity distribution at non-dimensional time 40. The time history of fluid forces around the body is plotted in Figure 32. Figure 33 shows the time history of vertical displacement and rotation. Figure 34 is the time history of vertical and rotation velocities of the body. The time history of the stability index compared with vertical displacement is shown in Figure 35. The behavior of the oscillating body based on 2DOF is more erratic than that based on the 1DOF. Constant stability is shown owing to the strong vertical and rotational elastic springs.

7.3. Stability analysis of 2DOF rectangular cylinder

The body is a rectangular prism. The parameters used are as follows: the mass of the quadrangular prism is 10.0, the non-dimensional spring constant in the y-direction is 10.0 and in the θ-direction it is 0.1; the structural damping coefficient is assumed to be 0.0. The time increment Δt is 0.02.

DOI: 10.1002/fld

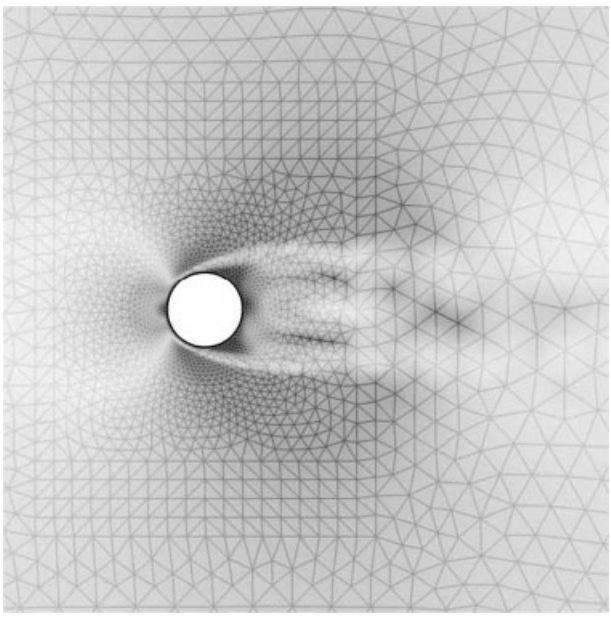

Figure 30. Velocity at time 10 (2DOF stable circular cylinder).

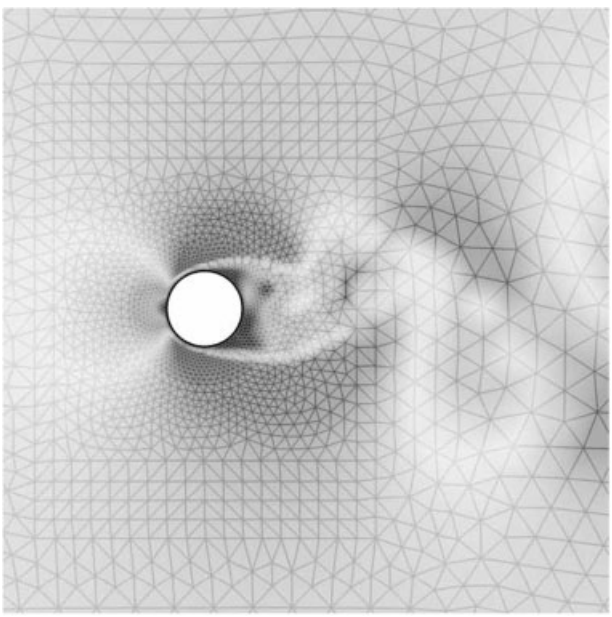

Figure 31. Velocity at time 40 (2DOF stable circular cylinder).

DOI: 10.1002/fld

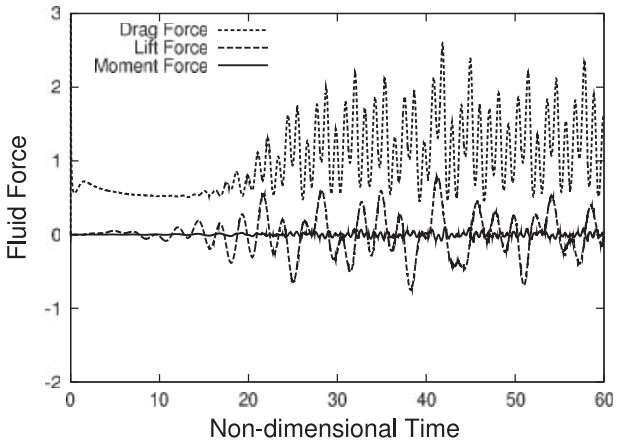

Figure 32. Fluid force *versus* time (2DOF stable circular cylinder).

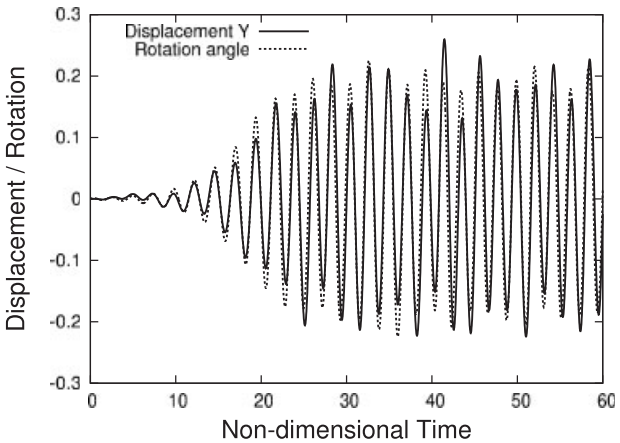

Figure 33. Displacement y and rotation angle of the body *versus* time (2DOF stable circular cylinder).

All values are non-dimensional. The computing time is 0.0–60.0 in non-dimensional time. Thus, the total energy is defined as follows:

$$E = \tfrac{1}{2} m V^2 + \tfrac{1}{2} k_y Y^2 + \tfrac{1}{2} I \dot{\Theta}^2 + \tfrac{1}{2} K_\theta \Theta^2 + E_p \tag{37}$$

and the stability index is

$$e = \left| \frac{\partial^2 E}{\partial \mathbf{X}_i \partial \mathbf{X}_j} \right| \tag{38}$$

DOI: 10.1002/fld

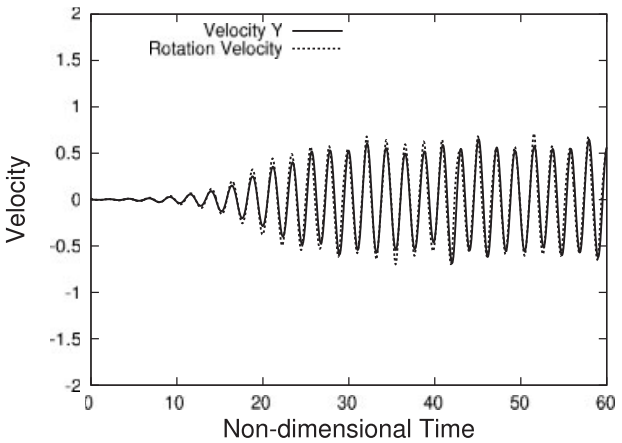

Figure 34. Velocity y of the body *versus* time (2DOF stable circular cylinder).

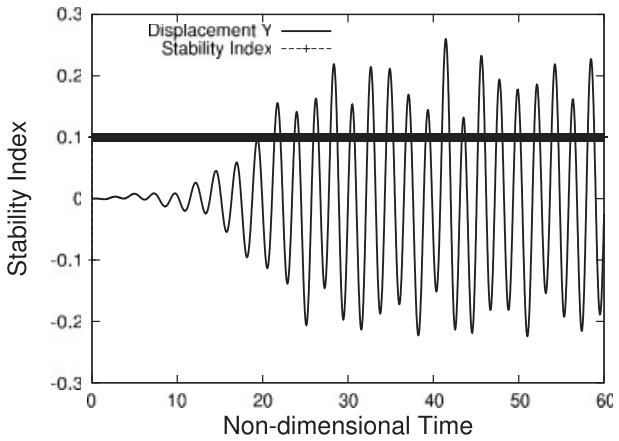

Figure 35. Stability index and y displacement of the body *versus* time (2DOF stable circular cylinder).

where

$$\mathbf{X}_i = \{x_1, x_2, x_3, \ldots, x_{\text{obj}}, y_1, y_2, y_3, \ldots, y_{\text{obj}}\} \tag{39}$$

in which $x_1, \ldots, x_{\text{obj}}, y_1, y_2, y_3, \ldots, y_{\text{obj}}$ are the coordinates on the surface node of the body. The computational domain and the finite element mesh are shown in Figures 36 and 37, where the mesh consists of 2396 nodes and 4602 elements, respectively. Computational conditions are also shown in Figure 36. The Reynolds number is 250.

The numerical results of the 2DOF rectangular cylinder are illustrated in Figures 38–43. Figure 38 represents velocity distribution at non-dimensional time 10. Figure 39 shows velocity distribution

DOI: 10.1002/fld

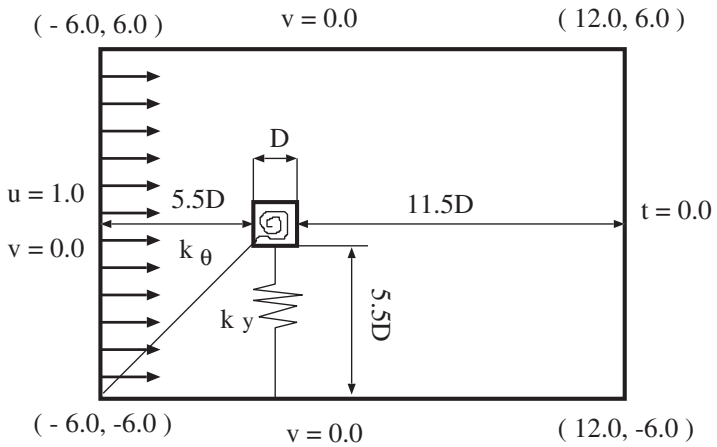

Figure 36. Computational domain.

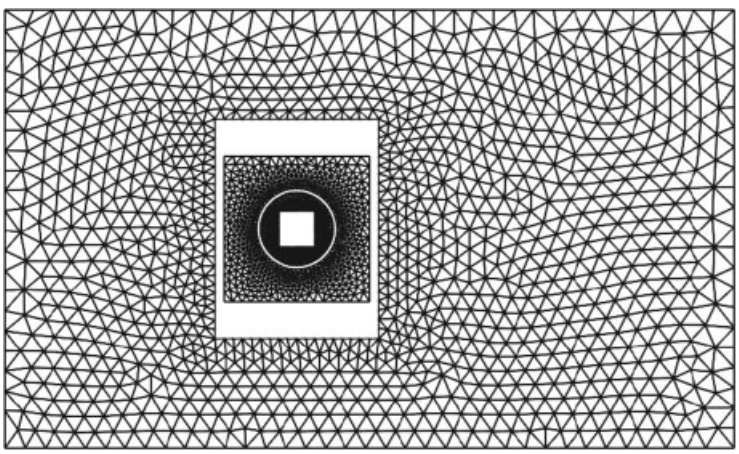

Figure 37. Finite element mesh.

at non-dimensional time 40. The time history of fluid forces around the body is plotted in Figure 40. Figure 41 shows the time history of vertical displacement and rotation. Figure 42 is the time history of vertical and rotation velocities of the body. The time history of the stability index compared with vertical displacement is shown in Figure 43.

The rectangular prism more easily oscillates in the rotational direction than the circular cylinder; hence, the amplitude of oscillation is magnified. In spite of a large amount of rotational oscillation and vertical displacement, the behavior of the body expressed by the stability index is stable. This result suggests that rotational oscillation may not significantly influence stability, although it depends on the body shape.

DOI: 10.1002/fld

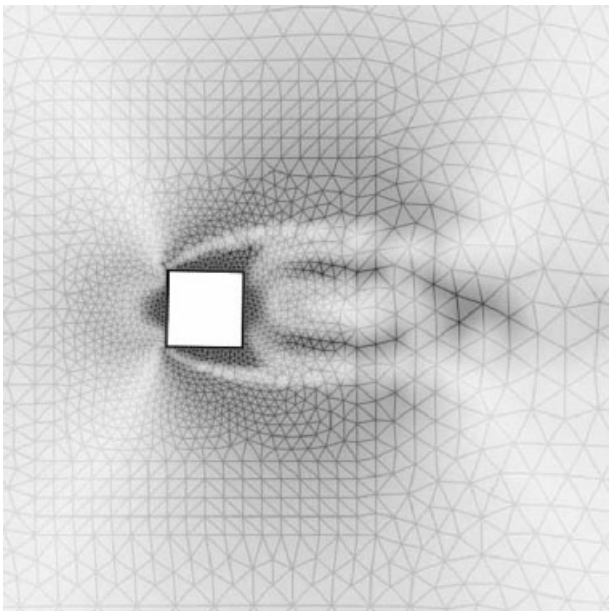

Figure 38. Velocity at time 10 (2DOF stable rectangular cylinder).

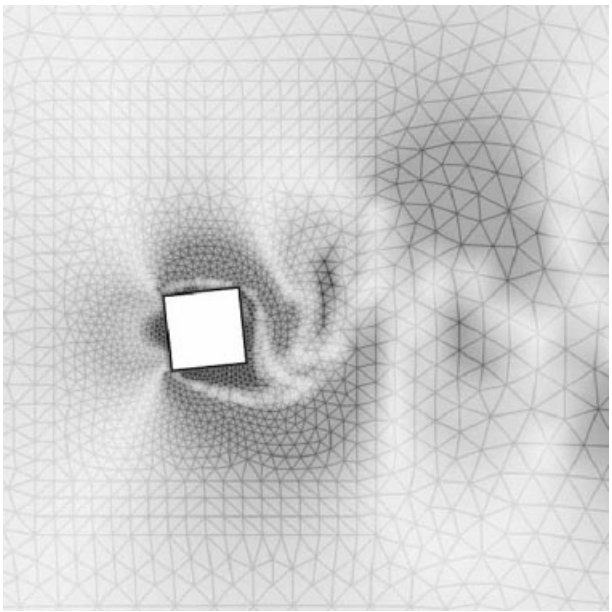

Figure 39. Velocity at time 40 (2DOF stable rectangular cylinder).

DOI: 10.1002/fld

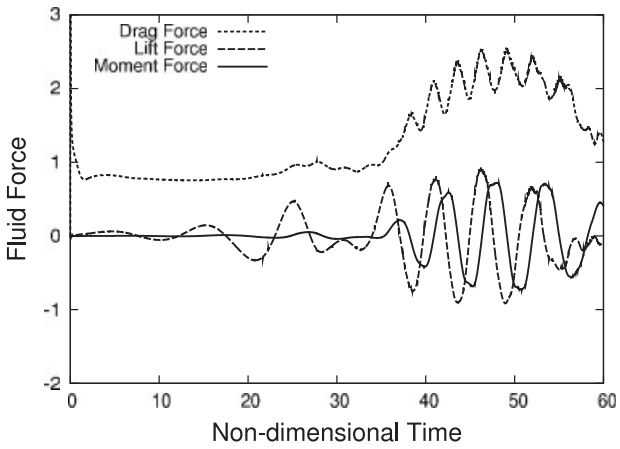

Figure 40. Fluid force *versus* time (2DOF stable rectangular cylinder).

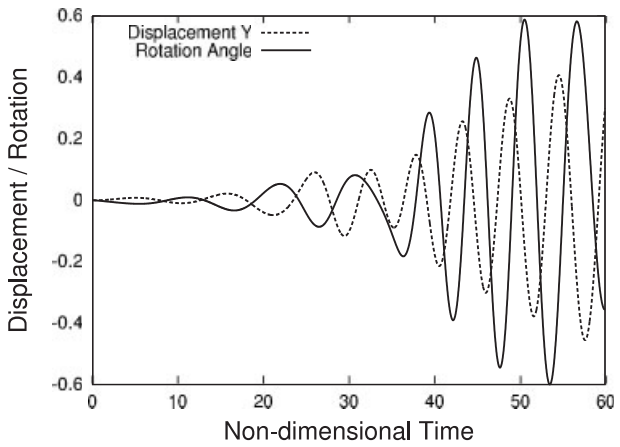

Figure 41. Displacement y of the body *versus* time (2DOF stable rectangular cylinder).

8. CONCLUSION

The stability of an oscillating body subjected to fluid forces was analyzed using ALE-FEM as a moving boundary problem and using SOAD for stability analysis. It is mentioned that accurate differentiation value by AD is reflected in the body stability of the behavior. These results can be understood as including that the behavior of the stability index can predict the behavior of the body. In the stability analysis of the 1DOF circular cylinder, three stability patterns of the oscillating body, i.e. a perfectly stable, neutral oscillating and unstable states, are exhibited. In the stability analysis of the 2DOF circular and rectangular cylinders, the stability of more complex oscillation phenomena can be predicted by the stability index. From these results, it is

DOI: 10.1002/fld

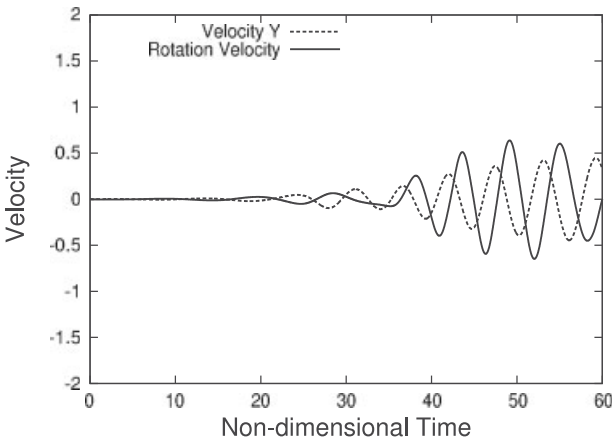

Figure 42. Velocity y of the body *versus* time (2DOF stable rectangular cylinder).

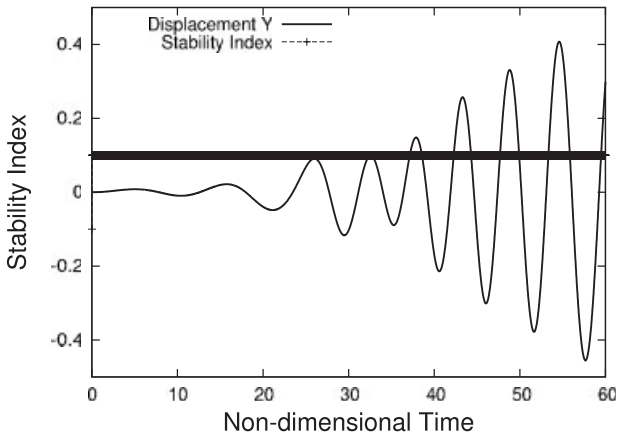

Figure 43. Stability index and y displacement of the body *versus* time (2DOF stable rectangular cylinder).

seen that the body's stability can be analyzed using the present method, provided AD can be used.

REFERENCES

1. Ding Y, Kawahara M. Secondary instability of wakes of a circular cylinder using finite element method. *International Journal of Computational Fluid Dynamics* 2003; **13**:279–301.
2. Ding Y, Kawahara M. Linear stability of incompressible fluid flow using a mixed finite element method. *Journal of Computational Physics* 1998; **139**(2):243–273.
3. Ding Y, Kawahara M. Linear stability of incompressible fluid flow in cavity using finite element method. *International Journal for Numerical Methods in Fluids* 1998; **27**(1–4):139–157.
4. Tezduyar TE *et al.* Flow simulation and high performance computing. *Computational Mechanics* 1996; **18**: 397–426.

DOI: 10.1002/fld

5. Kuhl E, Hulshoff S, de Borst R. An arbitrary Lagrangian Eulerian finite-element approach for fluid–structure interaction phenomena. *International Journal for Numerical Methods in Engineering* 2003; **57**:117–142. DOI: 10.1002/nme.749.
6. Donea J, Huerta A, Ponthot J-Ph, Rodriguez-Ferran A. Arbitrary Lagrangian–Eulerian methods. *Encyclopedia of Computational Mechanics*, Stein E, de Borst R, Hughes TJR (eds). Wiley: 2004.
7. Nomura T, Iijima M. A finite element procedure for viscous fluid–structure interaction problems using the arbitrary Lagrangian–Eulerian formulation. *Journal of the Japan Society of Civil Engineers* 1990; **417**(I–13):285–294.
8. Anderson RW, Pember RB, Eliott NS. An arbitrary Lagrangian–Eulerian method with local structured adaptive mesh refinement for modeling shock hydrodynamics. *Aerospace Science Meeting and Exhibition*, Fortieth American Institute of Aeronautics and Astronautics, Reno, NV, 14–17 January 2002.
9. Watanabe H, Sugiura S, Kafuku H, Hisada T. Multiphysics simulation of left ventricular filling dynamics using fluid–structure interaction finite element method. *Biophysical Journal* 2004; **87**(3):2074–2085.
10. Matsumoto J, Umetsu T, Kawahara M. Stable shape identification for fluid–structure interaction problem using MINI element. *Journal of Applied Mechanics* 2000; **3**:263–274.
11. Matsumoto J, Umetsu T, Kawahara M. Incompressible viscous flow analysis and adaptive finite element method using linear bubble function. *Journal of Applied Mechanics* 1999; **2**:223–232.
12. Tezduyar TE. Stabilized finite element formulations for incompressible flow computations. *Advances in Applied Mechanics* 1992; **28**:1–44.
13. Behr M, Tezduyar T. The shear-slip mesh update method. *Computer Methods in Applied Mechanics and Engineering* 1999; **174**:261–274.
14. Pironneau O. *Consistent Approximations*, *Automatic Differentiation and Domain Decomposition for Optimal Shape Design*. International Series, Mathematical Sciences and Applications, vol. 16, *Computational Methods for Control Application* 2001; 167–178.
15. Aubert P, Di Cesare N, Pironneau O. *Automatic Differentiation in C++ using Expression Template and Application to a Flow Control Problem*. *University of Paris 6*, 1999.